Received: 22 February 2022 | Accepted: 10 May 2022

DOI: 10.1002/maco.202213116

ARTICLE

Materials and Corrosion

Corrosion mechanisms of AZ31 magnesium alloy: Importance of starting pH and its evolution

Loic Prince[1] | Xavier Noirfalise[2] | Yoann Paint[2] | Marjorie Olivier[1,2]

[1]Materials Science Department, UMONS-University of Mons, Mons, Belgium

[2]Materia Nova asbl, Mons, Belgium

Correspondence
Loic Prince, Materials Science Department, UMONS-University of Mons, Place du parc 20, B-7000 Mons, Belgium.
Email: loic.prince@umons.ac.be

Funding information
Gouvernement Wallon; European Regional Development Fund

Abstract

This article aims at improving the understanding of the corrosion mechanism of AZ31 magnesium alloys during a long period of immersion in an aqueous electrolyte. In particular, the influence of the starting pH of the electrolyte on the oxidation of AZ31 alloy and its evolution due to corrosion phenomena were investigated. Several electrolytes with different pH values containing or not chlorides were used. The electrochemical properties of the metal substrate in these electrolytes were studied as a function of immersion time by electrochemical impedance spectroscopy. The kinetics of the reactions were determined by potentiodynamic polarization as well as dihydrogen evolution measurements by eudiometry. All these tests were carried out while the sample surface and electrolyte volume remained constant. The corrosion products generated on the alloy surface were analyzed by X-ray photoelectrons spectrometry. This study has shown that the evolution of the corrosion rate and the corrosion products depends greatly on the initial pH and the nature of the used electrolyte. Alkaline electrolyte leads to a passive protective layer that can be locally destroyed by chloride ions. For a neutral chloride electrolyte, the strong increase of the pH due to the magnesium corrosion is not able to form a protective layer by precipitation of corrosion products. The kinetic and the corrosion extent are affected by the pH changes.

KEYWORDS

corrosion, electrochemical techniques, electrolyte, magnesium alloy

1 | INTRODUCTION

Nowadays, magnesium is recognized as having a significant industrial potential due to the increasing demand for lightweight portable devices and transportation. Magnesium is one of the most abundant elements in the earth's crust. It can be found in different chemical forms: $MgCO_3$, MgO, $MgSO_4$ and different silicates. Magnesium is the lightest engineering metal with a density of 1.7 g/cm^3, which is significantly lower than aluminium (2.7 g/cm^3), titanium (4.5 g/cm^3) and iron (7.9 g/cm^3). In addition, it has other interesting properties such as high thermal conductivity, protection against electromagnetic damping, easy machinability and recyclability.[1] However, magnesium alloys are limited in their uses by high chemical reactivity and low corrosion resistance in aggressive environments.[2] The role of the intermetallic phases on the corrosion behaviour has been described in terms of their nobility and the microstructure of AZ31 has been fully studied.[3] The Al–Mn phase, which is dispersed both in the α-Mg phases and at grain borders as particles of average size between 2 and

20 μm, is the most common type of intermetallic found in AZ31 alloy.[4]

The standard potential of magnesium (−2.37 V/NHE) is very low. In the absence of water, magnesium reacts instantaneously with air to form a magnesium oxide layer [Equation (1)].[5,6]

$$Mg(s) + 1/2\ O_2 \rightarrow MgO\ (s). \quad (1)$$

Refson et al.[7] studied the chemisorption of water on MgO and showed that adsorbed water molecules are dissociated to form OH^- and H_3O^+, which leads to hydroxylation of the MgO surface.

$$MgO(surface) + H_2O(g) \rightarrow Mg(OH)_2(surface). \quad (2)$$

The hydroxylation of MgO film then leads to the formation of a bilayer structure of inner MgO (2–7 nm) and thicker outer porous $Mg(OH)_2$ layers [Equation (2)].[8–11]

The Pourbaix diagram indicates that the stability range of magnesium is below that of water by approximately 2 V. This means that magnesium is not stable in the presence of water.[12] Thus, several chemical forms of magnesium can appear depending on the solution pH. Magnesium is oxidized to Mg^{2+} in acidic or neutral media. In alkaline media, the formation of a protective $Mg(OH)_2$ film is thermodynamically stable according to the following reaction):

$$Mg + 2H_2O \rightarrow Mg(OH)_2 + H_2. \quad (3)$$

Nevertheless, the passive layer formed is not sufficiently protective, showing a Pilling-Bedworth ratio of 0.81 for MgO/Mg.[13] This value less than 1 indicates that the surface oxide layer is porous. The corrosion reaction of magnesium can be stated as the sum of the following redox reactions:

$$Mg \rightarrow Mg^{2+} + 2e^-, \quad (4)$$

$$H_2O + 2e^- \rightarrow H_2 + 2OH^-, \quad (5)$$

$$2H^+ + 2e^- \rightarrow H_2. \quad (6)$$

These reactions are representative of corrosion phenomena taking place when magnesium is exposed to an aqueous medium and are related to the distribution of Mg^{2+} ions and OH^- on the surface. The cathodic sites are characterized by a water reduction reaction and a dominance of OH^- and alkaline pH values, while the anodic sites have an acidic pH and high Mg^{2+} ion activity due to the anodic dissolution of magnesium.[14] In unbuffered chloride solution, the local pH on the Mg surface rapidly increases to 10.3 and stabilizes due to the low solubility of $Mg(OH)_2$.[15]

At low pH, the passivation film will be much less protective than that formed in an alkaline solution.[16] The surface films are mainly composed of $Mg(OH)_2$ in both neutral[17–19] and alkaline[5] solutions. The corrosion resistance differs with the electrolyte pH due to the possibility to form a different thickness of the MgO inner layer.[5] Recently, Wang et al.[20] studied the surface film on HP-Mg at different pH of a NaCl solution. The electrochemical measurements demonstrate the different corrosion activity in the different electrolyte pH. Interestingly, the thickness of the layer formed on Mg at pH 3 was more important than the film formed at pH 5.6 and 11. This phenomenon is explained by a strong local alkalinization of the surface and high consumption of oxygen near the surface. The MgO film is considered to provide some protection. The $Mg(OH)_2$ on the top is fluffy and porous and provides little protection.

The influence of the electrolyte pH is a phenomenon known in the literature. However, the impact of the initial pH seems to be a determining factor in the corrosion evolution of the corrosion on the sample and the stability of the passive layer. Nowadays, no study has demonstrated this phenomenon in the AZ31 magnesium alloys.

This study focuses more specifically on the influence of the initial pH of the electrolyte on the dissolution of AZ31 on the extent of corrosion and on the modification of this pH due to corrosion phenomena. Three electrolytes with two different pH values containing or not chlorides in alkaline media are used. The electrochemical activity of the AZ31 alloy in these electrolytes is studied as a function of immersion time by electrochemical impedance spectroscopy. The kinetics of the reactions are determined by potentiodynamic polarization as well as by measurements of dihydrogen evolution by eudiometry. To obtain similar information on the kinetics of the events, all the experiments are carried out while keeping the sample surface and the electrolyte volume constant. X-ray photoelectron spectroscopy (XPS) is used to examine the corrosion products that occur on the surface of the alloy.

2 | EXPERIMENTAL

2.1 | Materials and sample preparation

AZ31 magnesium alloy sheets were supplied by KG Fridman AB and have the following composition: 2.5%–3.5% Al, 0.7%–1.3% Zn, 0.2% Mn, 0.05% Cu, 0.04%

Ca, 0.0005% Fe, 0,1% Ni (wt%) and Mg balance. The samples were degreased by using 1 M NaOH and etched by immersion in two nitric acid solutions[21]: 2 M HNO_3 solution for 30 s and 0.25 M HNO_3 solution for 60 s. The samples were finally rinsed with distilled water before air drying.

2.2 | Selection of different electrolytes

Three different electrolytes were selected to study the effect of the initial pH and the chloride presence on the corrosion propagation. The pH range was chosen according to the pH/potential diagram.[12] The pH of 5.6 is the natural pH taken by demineralized water in presence of the air atmosphere. Magnesium is in its active zone of corrosion at this pH value while pH 12 corresponds to the magnesium passivation zone. The electrolytes were left in the open air to study the behaviour under usual conditions. Table 1 shows the different compositions and the pH values of the electrolyte media.

2.3 | Morphology characterization

The morphology of AZ31 samples was analyzed using scanning electron microscopy (SEM) (Hitachi SU8020 with cold cathode) and coupled to an energy dispersive X-ray spectrometer analyzer (EDX) to determine the element distribution.

2.4 | Electrochemical measurements

A conventional three-electrode electrochemical cell was used, composed of an Ag/AgCl/KCl saturated reference electrode, a platinum counter-electrode and a working electrode, namely, the studied sample. The electrochemical cell was placed in a Faraday cage to minimize the external electromagnetic interference on the system.

All the electrochemical measurements were carried out using a Parsat Model 2273 controlled by Powersuite® software. The sample area is 7 cm^2 in each case and the electrolyte volume is 30 ml. This volume is low to evaluate the pH change on the corrosion progress.

Before measuring the polarization curves and electrochemical impedance spectra, the stability of the open circuit potential (OCP) of the samples in each medium is previously determined for 24 h of immersion.

Potentiodynamic polarization curves were performed in the different electrolyte media using a sweep rate of 50 mV/min and sweep range of ±250 mV starting from OCP. The corrosion current density i_{corr} (mA/cm^2) is estimated by Tafel extrapolation of the cathodic branch of the polarization curve and the thickness loss P_i (mm/year) is related to the average corrosion rate using[22]:

$$P_i = 22.85\, i_{corr}. \quad (7)$$

The corrosion resistance of the bare samples in the different electrolyte media was studied by using electrochemical impedance spectroscopy versus immersion time. Electrochemical impedance spectroscopy (EIS) spectra were determined in a frequency range from 100 kHz to 100 MHz. The EIS data at low frequencies (10^{-3}–10^{-2} Hz) are highly dispersed due to the quick dissolution of magnesium substrate resulting in nonstationarities.

The Commercial software ZSimpWin was utilized for analyzing the obtained impedance spectra.

All the electrochemical measurements were reproduced at least twice.

2.5 | pH measurements

The electrolyte pH during the sample immersion was measured by using a CG 840 pH meter from Schott with an H62 glass electrode from SI Analytics. The calibration was made using pH 4 and pH 7 buffer solutions supplied by VWR BDH-Prolabo. The measurements were produced for three samples.

2.6 | Hydrogen evolution

Hydrogen evolution experiments were carried out upon the 7 cm^2 area of AZ31 using eudiometers.[23,24] All tests were carried out for 24 h without interruption and the volume of hydrogen released was manually recorded. All experiments are conducted at room temperature and the volume of H_2 residing in the eudiometer and dissolved in the aqueous medium was not considered since the solubility of H_2 in water is about 0.0016 g/kg at room temperature at a pressure of 1 atm.

The simplest and the most basic determination of the corrosion rate is the metal mass loss rate, Δw (mg/cm^2/day).

TABLE 1 Composition and pH of different electrolyte media

Media	Initial pH	Composition
Natural pH chloride	5.6	0.1 M NaCl
Alkaline	12	0.01 M NaOH
Alkaline/chloride	12	0.1 M NaCl/0.01 M NaOH

This rate can be converted to an average corrosion rate V_W (mm/year) using the following formula[22]:

$$v_w = 3.65\,\Delta w/\rho, \tag{8}$$

where ρ is the density of the metal (g/cm^3). For Mg alloys, ρ is 1.7 g/cm^3 and Equation (9) becomes

$$v_w = 2.10\,\Delta w. \tag{9}$$

In the overall corrosion reaction of pure Mg, one molecule of hydrogen is released for each atom of Mg being corroded. One mole (24.31 g) of metallic Mg corrodes for every mole [22.4 L at standard temperature and pressure conditions (0°C under 1 atm)] of hydrogen gas produced. Therefore, the rate of hydrogen production V_H (ml/cm^2/day) is related to the rate of metal weight loss, Δw (mg/cm^2/day) by following by formula:

$$\Delta w = 1.085\,V_H. \tag{10}$$

The corresponding corrosion rate V_{corr} (mm/year) is estimated by substituting Equation (10) into Equation (8) to give Equation (11):

$$V_{corr} = 2.279\,V_H. \tag{11}$$

2.7 | X-ray photoelectron spectrometry

AZ31 samples were washed with demineralized water and dried with a compressed air system after 7 days of immersion in different electrolyte media. XPS analyses were performed with a PHI VERSAPROBE 5000 spectrometer. The measurements were carried out employing an X-ray source with a spot size of 200 μm and the power of the source fixed at 50 W. After energy calibration using the C 1s reference peak at 285 eV, all spectra were plotted. The areas of the photoelectron peaks were calculated after subtracting a continuous background approximated by a Shirley baseline.

3 | RESULTS

3.1 | Microstructure of AZ31 alloy

The microstructure of AZ31 sample and the EDX spectra are identical to the microstructure obtained in our previous study[25] (Figure 1).

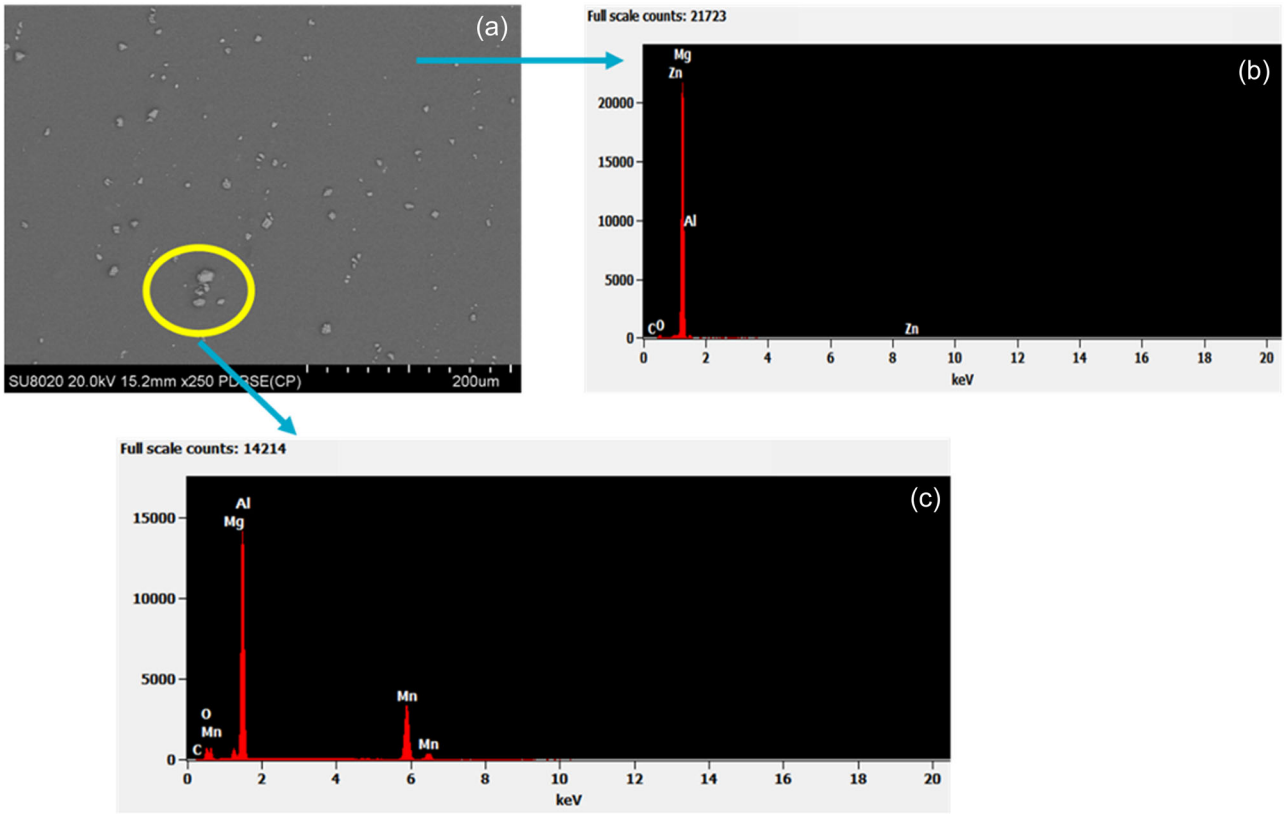

FIGURE 1 Microstructure of AZ31 by scanning electron microscope and composition of energy dispersive X-ray spectroscopy. [Color figure can be viewed at wileyonlinelibrary.com]

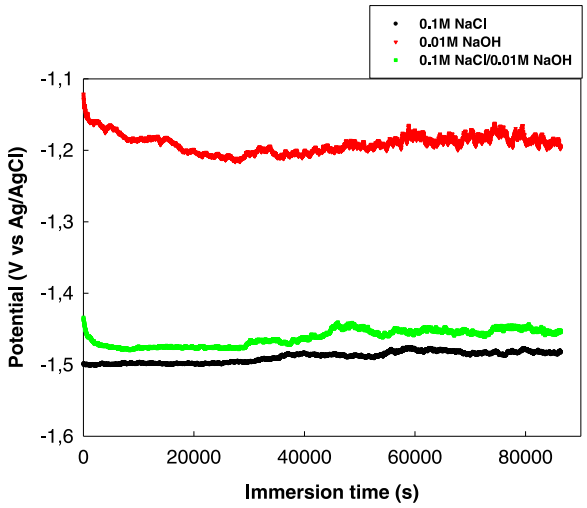

FIGURE 2 Variation in open circuit potential of AZ31 samples immersed in different electrolyte media. [Color figure can be viewed at wileyonlinelibrary.com]

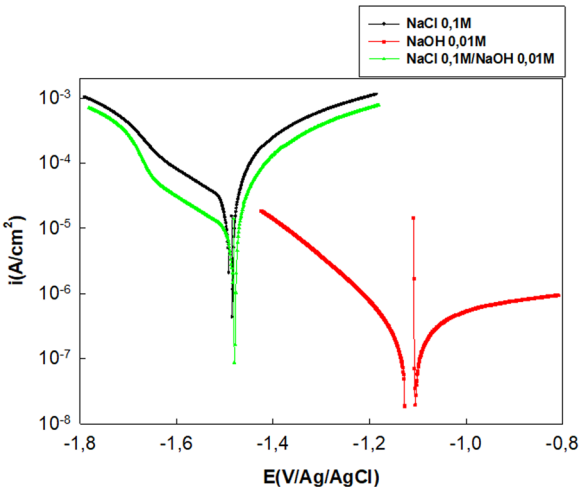

FIGURE 3 Anodic and cathodic polarization curves of AZ31 immersed for 6 h in 0.1 M NaCl, 0.01 M NaOH and 0.1 M NaCl/0.01 M NaOH solution. [Color figure can be viewed at wileyonlinelibrary.com]

This micrograph clearly shows the presence of intermetallic compounds. The Al remains in solid solution in the majority α phase, together with the alloyed Zn. The main type of intermetallic present in the AZ31 alloy is the Al–Mn phase dispersed both in the α grains and at the grain boundaries as inclusions of size between 2 and 20 μm.[4]

3.2 | Electrochemical measurements

3.2.1 | OCP

Before starting an electrochemical study of the corrosion behaviour of the sample in the different electrolytes, the OCP must be previously measured to verify its stability. The evolution of the OCP is followed during a prolonged immersion of 24 h (Figure 2).

The OCP for AZ31 samples in 0.1 M NaCl solution stabilizes around −1.50 V after a few minutes. During this period, a slight increase in potential up to −1.49 V is observed. In 0.01 M NaOH solution, the OCP is relatively stable at around −1.12 V after a few hours. Compared to the chloride-containing solution, the substrate immersed in 0.01 M NaOH has a more noble potential. The addition of chloride affects the passivation layer resulting in a decrease of potential (−1.46 V), a value slightly nobler than the potential of AZ31 immersed in NaCl. Furthermore, the presence of NaOH and NaCl causes instabilities in the curves reflecting the dynamic nature of a competitive process between corrosion and the tendency to passivate the surface. The electrochemical measurements were carried out after 6 h of immersion to ensure that a stable OCP value is reached.

3.2.2 | Potentiodynamic polarization

Potentiodynamic polarization measurements were carried out to study the anodic and cathodic behaviours in the different solutions. Figure 3 shows the polarization curves of AZ31 samples obtained after 6 h of exposure to 0.1 M NaCl, 0.01 M NaOH and 0.1 M NaCl/0.01 M NaOH.

To compare the three media, an extrapolation of the linear part of the cathodic curve is performed.[26] A significant decrease in the current densities (i) of the anodic and cathodic branches is clearly observed in the nonchlorinated alkaline medium which induces a significant decrease in the corrosion current densities. The corrosion current density is the order of 5.10^{-7} A/cm^2, whereas, in the presence of a 0.1 M NaCl solution, it is 10^{-4} A/cm^2. Furthermore, in a nonchlorinated alkaline environment, the corrosion potential shifts to more anodic values of the order of −1.12 V and anodic passive behaviour can be observed. In the case of the cathodic curve in a 0.01 M NaOH medium, only the water reduction could be identified as a cathodic reaction. With further polarization of the cathodic potential, a gradual increase in the cathodic current density is observed, indicating an increase in the reaction rate of hydrogen production. The addition of chloride ions in an alkaline environment leads to an increase in the corrosion current by a factor of 100. This means that the chloride ions penetrate the passivation layer and destabilize it, leading to an acceleration of the corrosion. The corrosion rates P_i (mm/year) are determined from the experimental results and are presented in Table 2.

3.2.3 | EIS

Figure 4 shows the Bode diagrams of the AZ31 alloy immersed in a 0.1 M NaCl solution for a period of 7 days.

From the Bode diagram obtained for the AZ31 samples immersed in 0.1 M NaCl (Figure 4), it appears that the impedance modulus at low frequency (10^{-1} Hz) remained low with immersion time varying from 1.10^3 to 9.10^3 Ω cm^2. These variations are associated with the instability of the magnesium oxide/hydroxide layer subjected to simultaneous growth and dissolution phenomena. Furthermore, regardless of the immersion time, two time constants could be observed in the Bode phase angle diagrams, the first in the middle-frequency range and the second in the low-frequency range. The first time constant could be associated with the response of the charge transfer resistance and the double-layer capacitance at the metal/solution interface, as it has a phase angle value of (−40° to −60°) characteristic of this capacitive behaviour.[27] Nevertheless, several studies show that the middle frequency time constant is associated with charge transfer but that the capacitance is mainly related to the very thin MgO oxide film present on the surface.[20,28] Indeed, Leleu et al.[28] studied the electrochemical behaviour of the WE43 alloy as well as pure Mg in a Na_2SO_4 solution. From the analysis of the high-frequency part of the impedance diagrams, using the complex capacitance plot, the thickness of the film was determined. The study reveals that the oxide film was 35% thinner on WE43 than on pure Mg in the Na_2SO_4 solution.[28] Furthermore, the increase in this time constant over time can be associated with the growth of corrosion products. It should be noted that the outer layer of the corrosion products from aqueous exposure is mainly Mg $(OH)_2$ as the dissolution of Mg favours the production of OH^- ions from the cathodic reaction. Nevertheless, Feliu et al.[27] have shown that CO_2 could dissolve in solution and cause the appearance of $MgCO_3$. The time constant at a low frequency (about 20°) corresponds to an inductive loop.[29] According to the literature,[30–34] this loop is attributed to the high concentration of magnesium ions in relatively film-free areas or to an intermediate step in the corrosion process involving the presence of adsorbed species on the surface, such as $Mg(OH)^+_{ads}$, $Mg(OH)_{2\,ads}$ and Mg^+_{ads}.[34] Although this approach is formally correct and provides an interpretation of the EIS response, recent experimental work has failed to experimentally reveal the presence of monovalent magnesium.[35,36] Gas-phase studies have indicated that the uni-positive Mg^+ reacts with water in milliseconds. There is no expectation that Mg^+ can exist in an aqueous solution for a time greater than several milliseconds.[37]

TABLE 2 Corrosion rate (P_i) of the AZ31 immersed in the different electrolytic solutions measured by Tafel extrapolation

Electrolyte media	Corrosion rate (mm/year)
0.1 M NaCl	2.28
0.01 M NaOH	0.011
0.1 M NaCl/0.01 M NaOH	1.14

Figure 5 shows the Bode diagram of the AZ31 alloy immersed in the 0.01 M NaOH solution for a period of 7 days.

In the Bode diagrams (Figure 5) obtained for the samples immersed in a 0.01 M NaOH medium, the impedance modulus at low frequency is much higher than in the medium containing only chlorides. Indeed, the impedance modulus varies from 10^5 to 2.10^5 Ω cm^2. It can, therefore, be concluded that the passivation layer is stable in this pH range with a capacitive behaviour over a wide frequency range (−80°). It should be noted that there is a change in the time constants after 3 days of immersion. The main time constant is shifted at lower frequencies and an additional time constant appears at higher frequencies. This change can be associated with the increase in thickness of the passive film. The

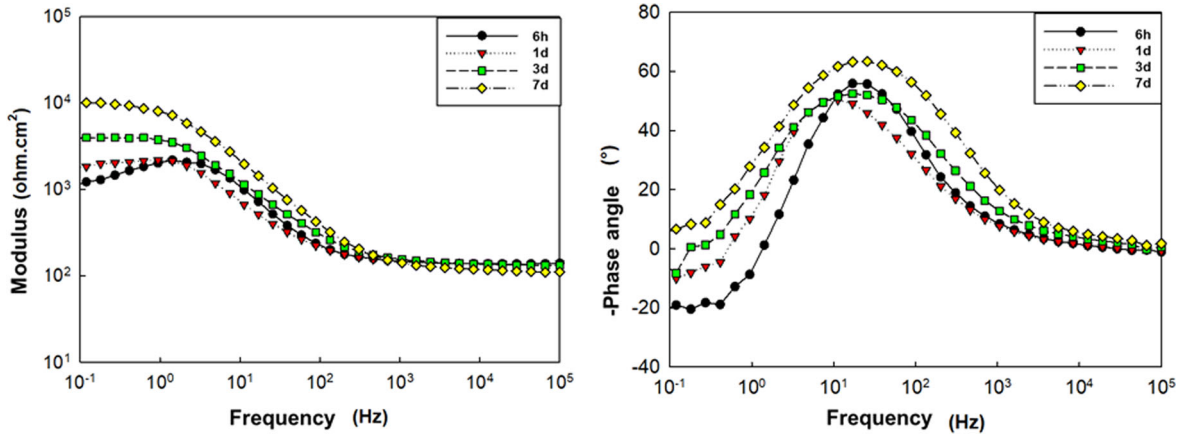

FIGURE 4 Modulus and phase angle Bode diagrams obtained for AZ31 immersed in 0.1 M NaCl for 7 days. [Color figure can be viewed at wileyonlinelibrary.com]

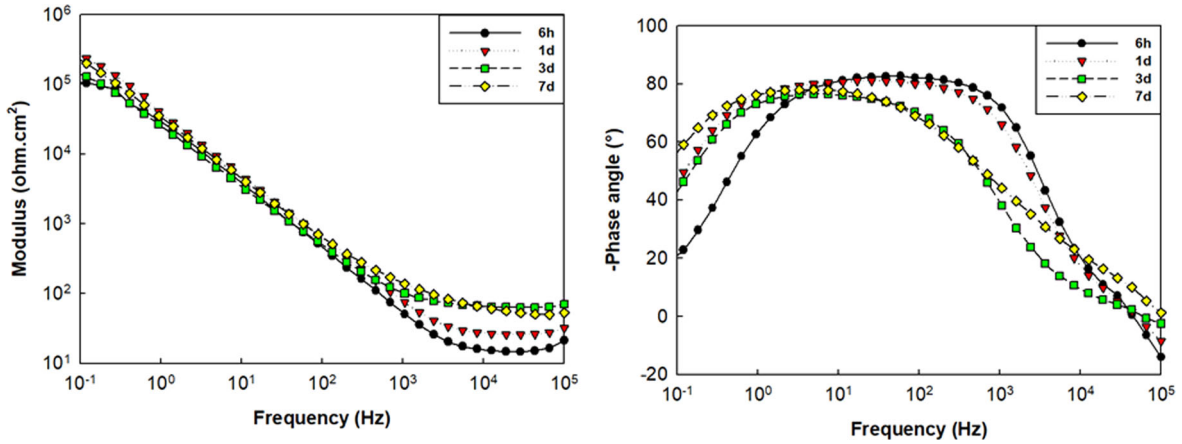

FIGURE 5 Modulus and phase angle Bode diagrams for AZ31 immersed in 0.01 M NaOH for 7 days. [Color figure can be viewed at wileyonlinelibrary.com]

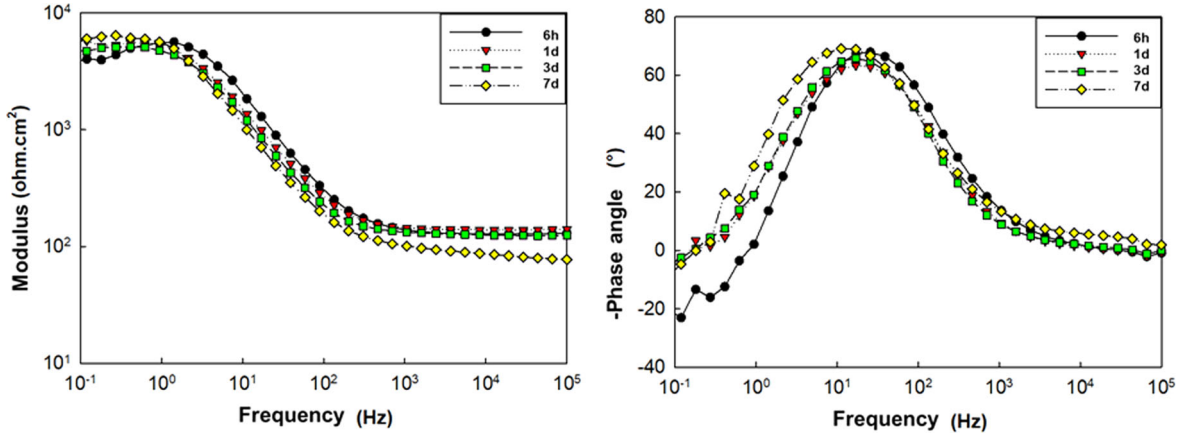

FIGURE 6 Modulus and phase angle Bode diagrams for AZ31 immersed in 0.1 M NaCl/0.01 M NaOH for 7 days. [Color figure can be viewed at wileyonlinelibrary.com]

inductive loop is not observed in this medium, which means that the corrosion kinetics are strongly reduced.

Figure 6 shows the Bode diagrams of the AZ31 alloy immersed in 0.1 M NaCl/0.01 M NaOH for 7 days.

In the Bode modulus diagrams (Figure 6) obtained for the samples immersed in 0.01 M NaOH/0.1 M NaCl, the impedance modulus at low frequency remains low as a function of immersion time. Nevertheless, the initial value is higher than in the neutral chloride medium, ranging from 4.10^3 to $9.10^3\ \Omega\,cm^2$. Furthermore, on the Bode phase plots, two time constants can be revealed, regardless of the immersion time, the first one being in the middle frequency range and the second one in the low-frequency range. The first is associated with the response of the passive layer of the substrate with a phase angle characteristic of a capacitive response (−70°). The extent of the time constant could also be related to the growth of the corrosion products. At low frequencies, an inductive behaviour caused by the evolution of superfluous hydrogen is detected. These results mean that despite the presence of the alkaline medium, chloride ions can destroy this protective layer.

To quantify the electrochemical parameters of the studied systems, the Bode diagrams were interpreted with equivalent electrical circuits that have an appropriate physical meaning. Based on the corrosion phenomena reflected in the EIS spectra, these were fitted by three different equivalent circuits (Figure 7).

In circuit a (Figure 7), R_s corresponds to the resistance of the electrolyte, CPE_{dc} is associated with the electrochemical double layer at the metal/solution interface in parallel with R_t which is the charge transfer resistance. This part of the circuit describes the dissolution of the AZ31 alloy. R is the resistor in series with the inductance L.[30] L represents the adsorption of intermediate species on the alloy surface.[29] CPE elements were used instead of pure capacitors to obtain a more accurate fitting by considering a possible nonideal behaviour of the system.

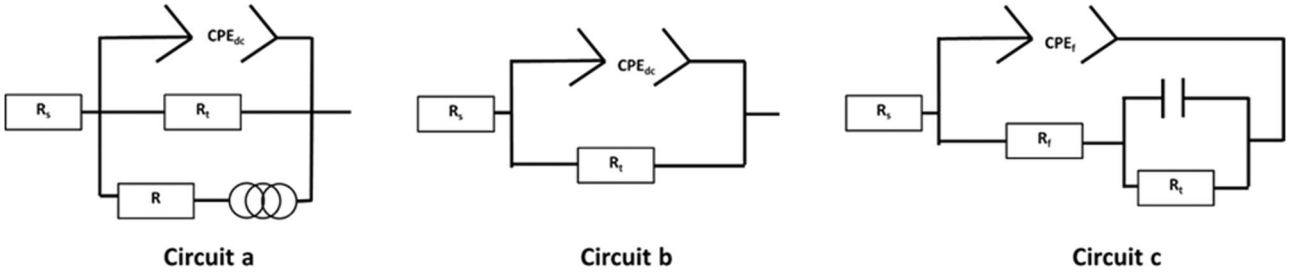

FIGURE 7 Equivalent electrical circuits to model Bode diagrams.

In the literature, the impedance of a CPE element is written as $Z_{CPE} = 1/(Q_0(i\omega)^n)$, where n is the frequency dispersion factor varying from 0 to 1. The CPE behaves as a resistor if $n = 0$ and as a pure capacitor if $n = 1$.[38] Circuit a is used to describe the behaviour observed in a chloride medium starting at natural pH. In circuit b (Figure 7), R_s, CPE_{dc} and R_t also correspond to the electrolyte resistance, the double-layer behaviour and the charge transfer, respectively. Nevertheless, based on the experimental results, it cannot be neglected that the CPE_{dc} is also a CPE_{ox} associated with the presence of an oxide layer.[20,28] This circuit is mainly used to describe the behaviour of the alloy immersed in alkaline solutions. Finally (Figure 7), in circuit c, an additional time constant is added to take into account the behaviour of the passive film formed in nonchloride alkaline medium after a long immersion time. CPE_f and R_f are the phase constant element and the resistance related to the capacitance and barrier properties of the film formed on the surface of the metal surface, respectively. Figure 8 shows the modeling results of the experimental data in Figures 4–6 using the circuits in Figure 7. The results are presented in Table 3.

Figure 9 shows the evolution of the charge transfer resistance in the different electrolyte media.

An increase in the charge transfer resistance R_t can be observed over the immersion time for the substrate immersed in a 0.1 M NaCl medium due to the growth of magnesium corrosion products and the local increase in pH. The R and L parameters also increase with immersion time. The inductive loop disappears after 3 days of immersion.

In the 0.01 M NaOH solution, the charge transfer resistance values are in agreement with the modulus values at low frequencies. In fact, the R_t values are stable with the immersion time confirming the protective behaviour of the passivation layer which remains stable in this environment. After 7 days, the appearance of a film resistance R_f is observed, indicating densification of the passivation layer during the immersion time.

In the 0.01 M NaOH + 0.1 M NaCl solution, the charge transfer resistance values are about two orders of magnitude lower than those obtained without chloride ions. The presence of the L and R parameters was necessary, as the inductive loop is present after 6 h of immersion. However, this time constant disappears for longer immersion times.

The CPE_{dc} values have orders of magnitude compatible with the physical meaning of an electrochemical double layer (10^{-5}–10^{-6} $Fcm^{-2}s^{n-1}$). It should be noted that the CPE_{dc} values for the NaOH solution are low (10^{-6} $Fcm^{-2}s^{n-1}$) to be assimilated to the capacitive double layer. It can be linked to the existence of a thin coating of MgO in this case. The values of n are higher than 0.75 and 0.9 for the neutral chloride medium and for the two alkaline media, respectively. The values are representative of a behaviour quite close to a pure capacitive one when a passive film is established.

3.3 | pH evolution

To understand the corrosion evolution of the AZ31 substrate, the evolution of the pH of the solutions as a function of the immersion time was recorded as shown in Figure 10.

For all three samples, the pH stabilizes between 10 and 11 after a few hours. In the case of the initial neutral medium containing chlorides, a sharp increase in pH is measured, reaching 10 after 1 h. The production of hydrogen and OH^- are always a sign of corrosion. Active corrosion of magnesium in an initially neutral pH induces a huge production of OH^- and so a sharp increase of pH till reaching the pH leading to the magnesium hydroxide precipitation due to its low solubility.[39] Thus, after immersion, the increase in pH of the medium leads to precipitation of corrosion products on the surface of the substrate.

In the case of the initial alkaline solutions with or without chloride ions, the pH decreases slightly with time, from 12 to 11.

In an alkaline environment, the slight decrease in pH is explained by two phenomena. First, at this pH, hydroxides are able to precipitate, leading to a

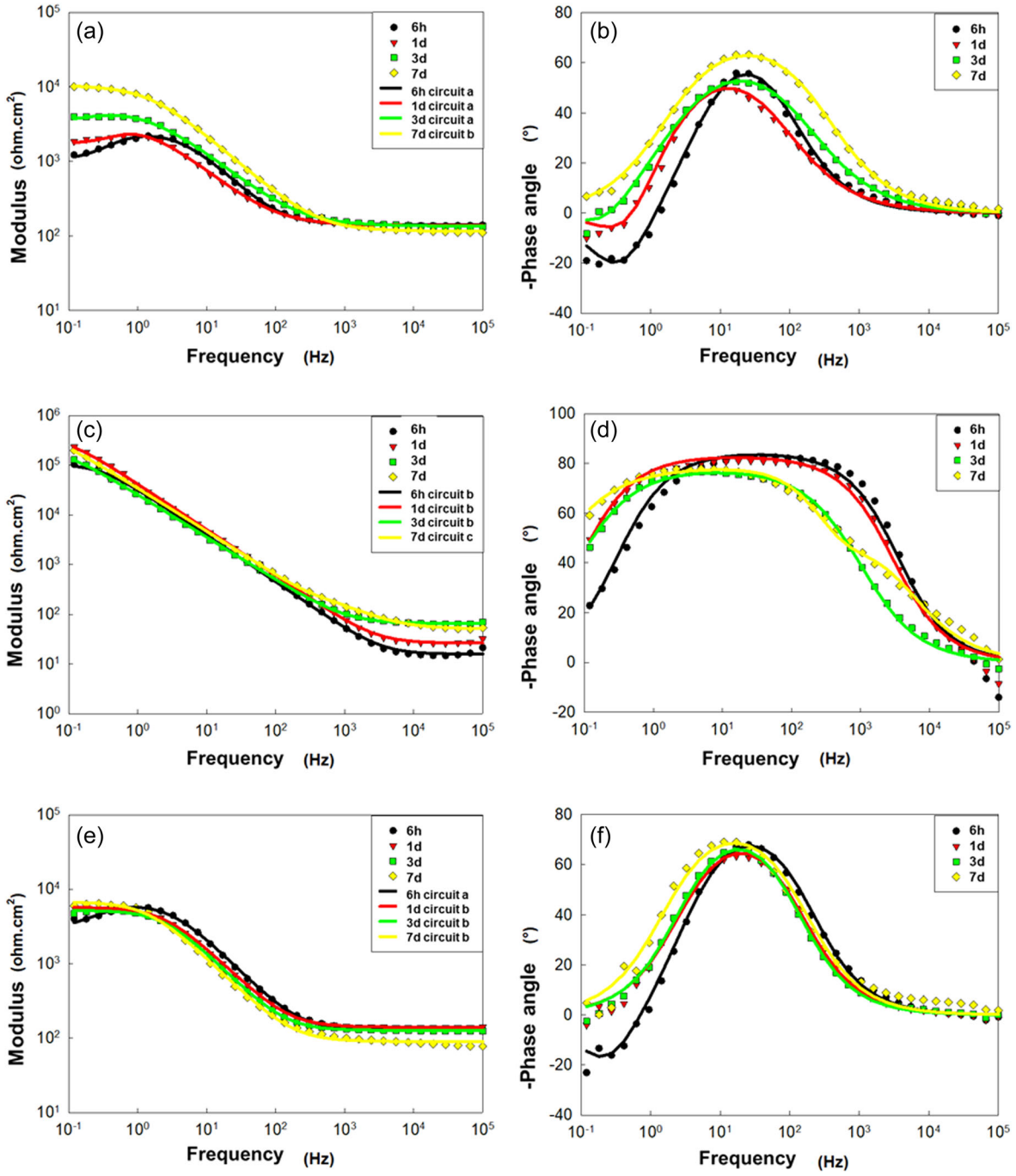

FIGURE 8 Impedance modulus (a,c,e) and phase angle (b,d,f) acquired during immersion of AZ31 in 0.1 M NaCl (a,b), 0.01 M NaOH (c,d), 0.1 M NaCl/0.01 M NaOH (e,f). [Color figure can be viewed at wileyonlinelibrary.com]

consumption of hydroxide ions in the solution.[40] In addition, as electrolytes are in contact with air, carbon dioxide can be dissolved in the electrolyte.[27] Given the alkaline pH, carbonate ions can consume magnesium ions and thus participate in the formation of magnesium carbonate.[25] Li et al.[41] showed that in slightly alkaline solutions (pH 11), significant corrosion occurs on the primary matrix. Minimal corrosion occurred on the β phase. The Al–Mn intermetallic served as strong cathodic sites with a local generation of H_2 bubbles. This phenomenon can also participate in the evolution of the solution pH.

3.4 | Hydrogen evolution

As already mentioned, magnesium alloy corrosion can be described as a redox process of oxidation of magnesium coupled with reduction and formation of H_2 from hydrogen ions and/or the hydrogen atom in the water

TABLE 3 Modelling results of electrochemical impedance spectroscopy spectra for AZ31 in different electrolytes as a function of immersion time

0.1 M NaCl	R_s (Ω cm^2)	CPE_{dc} ($Fcm^{-2}s^{n-1}$)	n	R_t (Ω cm^2)	L (Henry)	R (Ω cm^2)
6 h	141.8	1.93×10^{-5}	0.91	2217	1103	1542
1 days	138.4	$4.95 \times 10-^{5}$	0.79	2848	1664	3737
3 days	135.5	$3.07 \times 10-^{5}$	0.77	4814	9797	1.20×10^{4}
7 days	115.6	1.43×10^{-5}	0.82	1.05×10^{4}	/	/

0.01 M NaOH	Rs(Ω cm^2)	CPE_f ($Fcm^{-2}s^{n-1}$)	n	R_f (Ω cm^2)	CPE_{dc} ($Fcm^{-2}s^{n-1}$)	n	R_t (Ω cm^2)
6 h	15.7	/	/	/	5.1×10^{-6}	0.94	1.1×10^{5}
1 days	26.3	/	/	/	$4.3 \times 10-^{6}$	0.92	4×10^{5}
3 days	64.8	/	/	/	7.8×10^{-6}	0.86	2.5×10^{5}
7 days	50.7	4.98×10^{-6}	0.82	383	1.1×10^{-6}	1	3.3×10^{5}

0.1 M NaCl/ 0.01 M NaOH	R_s (Ω cm^2)	CPE_{dc} ($Fcm^{-2}s^{n-1}$)	n	R_t (Ω cm^2)	L (Henry)	R (Ω cm^2)
6 h	130.2	9.57×10^{-6}	0.93	5295	5514	5715
1 day	139.6	1.43×10^{-5}	0.90	5611	/	/
3 days	126.7	3.54×10^{-5}	0.92	5294	/	/
7 days	89.6	2×10^{-5}	0.90	5698	/	/

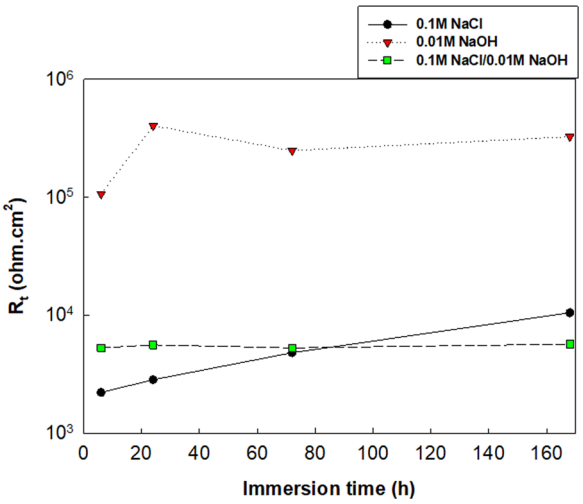

FIGURE 9 Evolution of the charge transfer resistance as a function of immersion time in the different electrolyte media. [Color figure can be viewed at wileyonlinelibrary.com]

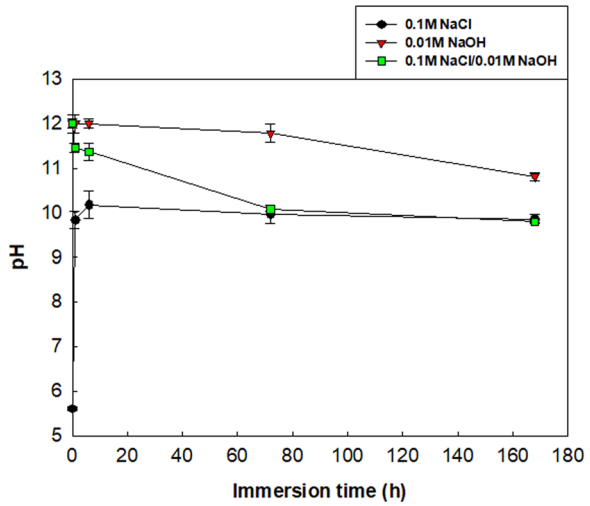

FIGURE 10 Evolution of the pH for the different electrolyte solutions. [Color figure can be viewed at wileyonlinelibrary.com]

molecule.[42] The overall reaction of the process can be written as follows:

$$Mg(s) + 2H_2O(l) \rightarrow Mg(OH)_2(aq) + H_2(g). \quad (12)$$

Theoretically, without taking into account the minor dissolution in the electrolyte, hydrogen can be directly used to calculate the consumption rate of Mg alloys.[24] For the study of the effect of pH in the different electrolyte media, the volume–time response of H_2 was recorded by eudiometry.

From the H_2 volume–time curves presented in Figure 11, it appears that the H_2 production shows an increase ranging from 0 to 8 ml in 24 h for the solution containing 0.1 M NaCl. This phenomenon is related to the strong oxidation of the magnesium surface which leads to high production of dihydrogen. Then, in

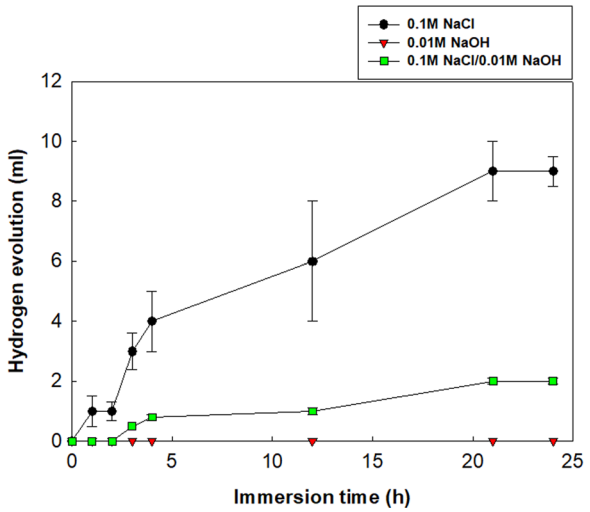

FIGURE 11 Evolution of the volume of dihydrogen as a function of immersion time in different electrolyte media. [Color figure can be viewed at wileyonlinelibrary.com]

TABLE 4 Corrosion rate (V_{corr}) of the AZ31 immersed in the different electrolytic solutions measured by a release of dihydrogen over a period of 24 h

Electrolyte media	Corrosion rate (mm/year)
0.1 M NaCl	2.93 ± 0.54
0.01 M NaOH	0 ± 0
0.1 M NaCl/0.01 M NaOH	0.48 ± 0.16

the case of the solution containing 0.1 M NaCl/0.01 M NaOH, there is a deceleration in the quantity of hydrogen produced. The alkalinity of the medium seems to inhibit the hydrogen production reaction. Finally, the medium containing only 0.01 M NaOH does not produce hydrogen or is in too small quantities to be detected and collected. The corrosion rates (V_{corr}) (mm/year) are determined from the experimental results and are presented in Table 4.

3.5 | Evolution of the corrosion product during immersion time

To confirm these results, optical images of the substrates were taken after different immersion times (Figure 12) in the three electrolytes.

As shown in Figure 12a, pitting appears on the surface after one immersion hour for the sample immersed in 0.1 M NaCl solution. Generalized corrosion of this sample is clearly observed for the longer immersion times (Figure 12b,c).

In 0.01 M NaOH solution (Figure 12d–f), the surface remains intact and seems visually insensitive to corrosion. This phenomenon is characteristic of substrate passivation.

Finally, in the alkaline medium containing chlorides (Figure 12g–i), localized corrosion is observed after 1 day with a progression under the form of filaments. Corrosion must be caused by the chloride ions breaking the passive film. Corrosion becomes generalized at 7 days of immersion. These results are in good agreement with the electrochemical measurements. These results confirm that even if the pH reaches a value of 10.3 after only 1 h of immersion in 0.1 M NaCl (solution 1) which is close to the pH of the two other solutions, the corrosion rate is significantly higher than for the two other electrolytes meaning that the initial pH has an important role on the critical effect of magnesium corrosion. Corrosion remains generalized with high hydrogen production.

3.6 | XPS

The XPS study was carried out to characterize the surface composition of AZ31 alloy exposed to air as well as immersed in the three selected media for seven immersion days.

The relative compositions of the extreme surface of AZ31 exposed to air and in the three electrolytes are determined by XPS analysis and are presented in Table 5.

Table 5 indicates that the surface exposed to air is mainly composed of magnesium, aluminium, zinc, manganese, carbon, oxygen and fluorine. This is in good agreement with the morphology of the surface studied by SEM.[25] The carbon and oxygen contents are very high compared to the other elements detected on the outer surface. This high level can be partly explained by the contamination of the surface by atmospheric pollution as well as the exposure to air which leads to oxidation of the surface.[19] The presence of fluorine is probably due to surface contamination from sample preparation before XPS analysis. Moreover, the percentage of aluminum detected in the spectrum is higher than its bulk content (3 at%). These figures tend to confirm, on the one hand, a nonuniform distribution of aluminum and magnesium and, on the other hand, a surface enrichment in Al of AZ31 alloy.[43]

The composition of the surface exposed to the 0.1 M NaCl electrolyte indicates the presence of magnesium, oxygen and carbon. In contrast to AZ31 exposed to air, the presence of elements such as aluminium or zinc from the substrate is not observed. This means that the XPS only distinguishes the corrosion product present on the surface of the sample.

The surface composition of the samples immersed in 0.01 M NaOH and 0.01 M NaOH/0.1 M NaCl indicate the

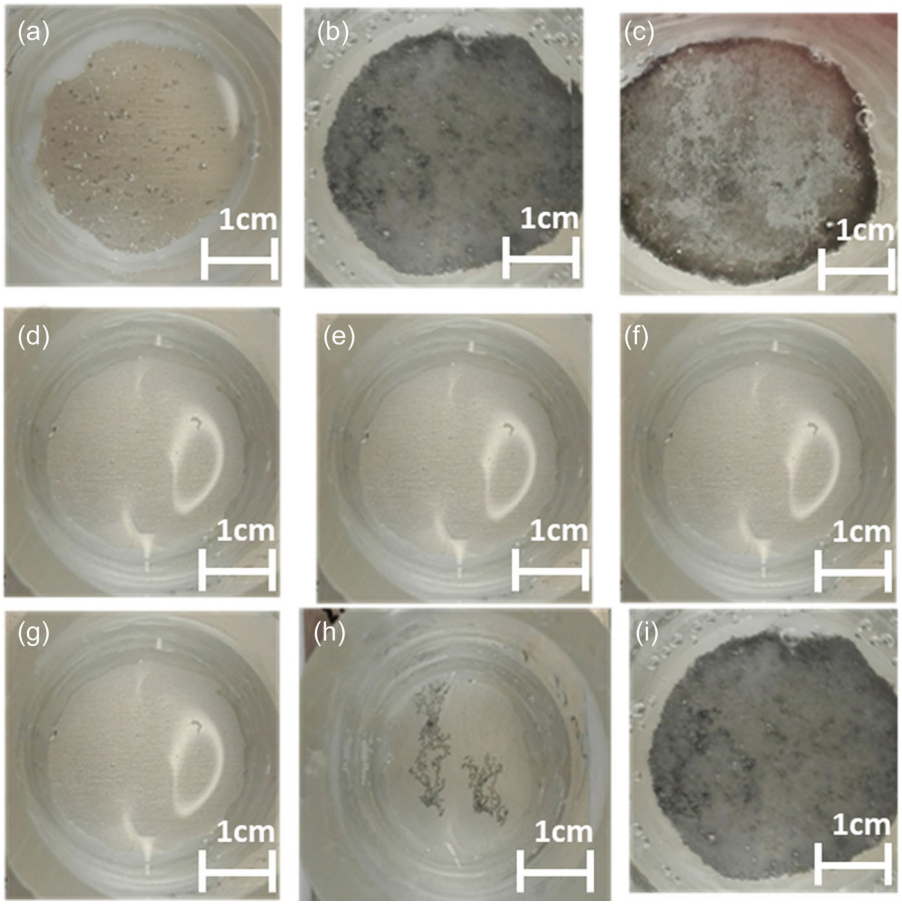

FIGURE 12 Optical images of AZ31 samples after immersion: (a) 1 h, (b) 1 day, (c) 7 days in 0.1 M NaCl, (d) 1 h, (e) 1 day, (f) 7 days in 0.01 M NaOH, (g) 1 h, (h) 1 day, (i) 7 days in 0.01 M NaOH/0.1 M NaCl. [Color figure can be viewed at wileyonlinelibrary.com]

TABLE 5 Relative composition of the outer surface of a sample exposed to air and immersed for 7 days in different electrolyte media

Element (atomic %)	C 1s	O 1s	Al 2p	Mg 2p	Zn 2p	Mn 2p	F1s	Na 1s
Exposed to the air	25	51.6	9.5	10.3	1	0.9	1.7	
0.1 M NaCl	8.4	63.5		28.1				
0.01 M NaOH	12.6	56.1	5.1	23				3.2
0.1 M NaCl/0.01 M NaOH	9.5	58.6	5	21.5				5.4

presence of magnesium, aluminum, carbon, oxygen and sodium. The carbon and oxygen contents are very high compared to the other elements detected on the surface. This rate is representative of the presence of passivation film on the surface of the sample. As far as sodium is concerned, it probably results from the presence of NaOH in the solution which impregnated the oxidized surface.

The chemical state of C 1s is studied and Figure 13 shows the results for samples immersed in different electrolyte media. Data of the components involved in the deconvolution of the C 1s photoelectrons peak of AZ31 immersed in different electrolytes (Table 6).

The C 1s peaks detected for binding energies of 284–289 eV (Figure 13) are often attributed to surface contamination upon exposure to air, while the highest binding energy near 290 eV is related to carbonate species. AZ31 exposed to air (Figure 13a) shows an atomic percentage of only 4.75 at% in carbonate relative to the carbon peak. An amount of 3.94 at% in carbonate is detected for the sample immersed in 0.1 M NaCl (Figure 13b) compared to the carbon peak. For the sample immersed in 0.01 M NaOH (Figure 13c), a second peak is present at 286.45 eV which is related to the presence of C–O binding as observed for AZ31 exposed to air. However, no carbonate could be identified in this sample. The presence of the MgO layer could prevent carbonate formation. Furthermore, the absence of chloride does not activate the dissolution of magnesium and therefore its possible reactivity with the carbonate dissolved in the solution. Finally, in the alkaline medium containing chlorides (Figure 13d), an atomic percentage of only 0.76 at% in carbonate compared to the carbon

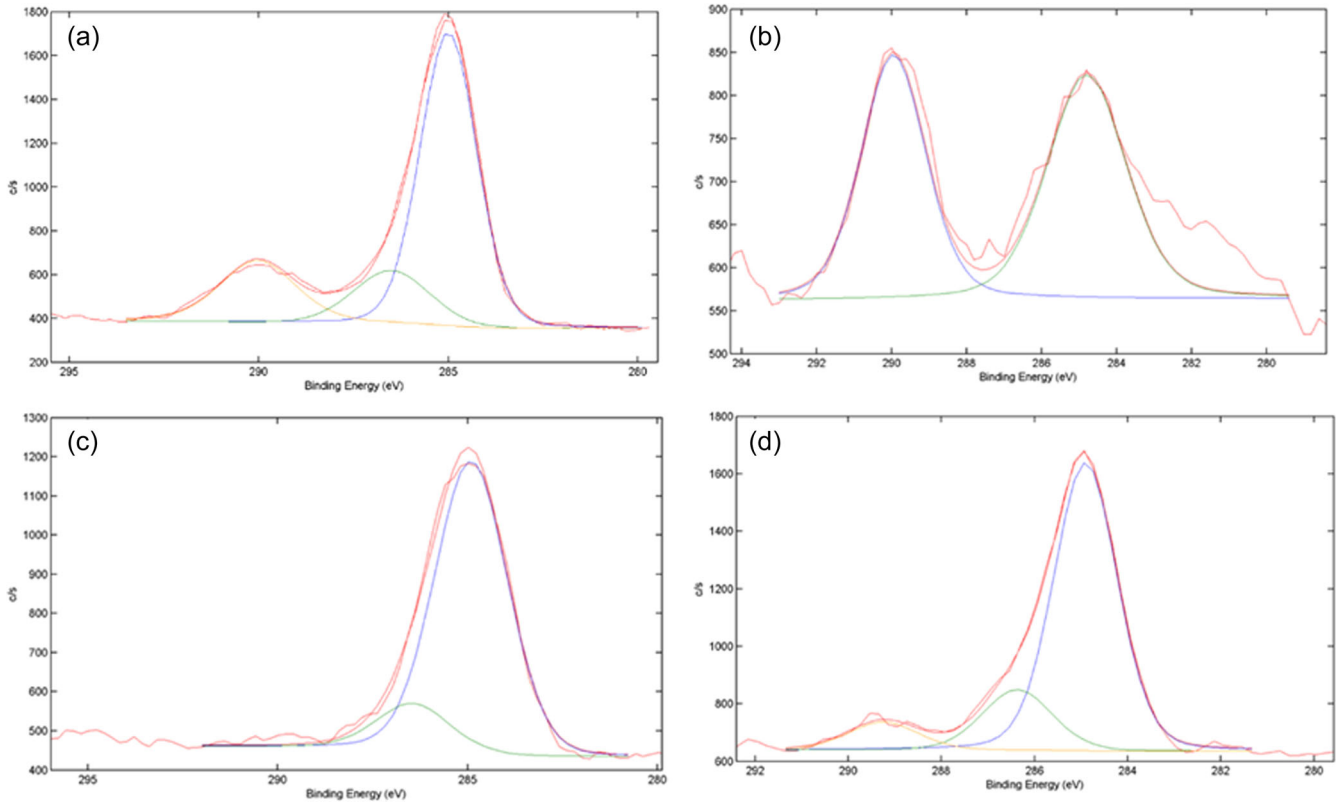

FIGURE 13 Chemical state obtained by X-ray photoelectron spectroscopy analysis of the C 1s spectrum for AZ31 exposed for 7 days: (a) to air, (b) 0.1 M NaCl, (c) 0.01 M NaOH, (d) 0.1 M NaCl/0.01 M NaOH. [Color figure can be viewed at wileyonlinelibrary.com]

TABLE 6 Data of the components involved in the deconvolution of the C 1s photoelectrons peak of AZ31 immersed in different electrolytes

Chemical bond (% relative)	C–C	C–O	CO_3^{2-}
Exposed to the air	64.4	15.7	19.9
0.1 M NaCl	52.9		47.1
0.01 M NaOH	86	14	
0.1 M NaCl/0.01 M NaOH	74.7	17.2	8.1

peak is measured. Such a low quantity confirms the hypothesis of surface pollution.

The chemical state of Mg is studied by analysis of Auger KLL spectra. Figure 14 shows the results for a sample immersed in the different electrolyte media.

The XPS spectrum of Mg 2p does not distinguish the contributions of Mg or oxidized Mg as the energies of the species are very close or even equal. To distinguish these species, the Auger Mg KLL spectra are analyzed (Figure 14). The position of the Mg KLL spectrum shows that it is in the oxidized form with an energy of 307.2 eV regardless of the medium.[18,44] After immersion in the different solutions, there is no change in the peaks.

4 | DISCUSSION

In the 0.1 M NaCl solution (pH 5.6), corrosion begins with the breakdown of the MgO layer leading to the formation of generalized corrosion and formation of the nonprotective layer of $Mg(OH)_2$. EIS measurements show a sharp decrease of the modulus at low frequencies during immersion time and are associated with an inductive behaviour. This phenomenon can be related to the dissolution and precipitation of corrosion products on the magnesium substrate. The pH of the solution strongly rises during the first hours of immersion. When the pH value reaches 10.5, the corrosion products of magnesium appear on the substrate as demonstrated by EIS and optical image. The presence of adsorbed species is related to the observation of the inductive loop on the Bode diagrams which can be associated to Mg^+_{ads} species.[29] Despite the appearance of this corrosion product ($Mg(OH)_2$), the dissolution of the substrate continues as shown by hydrogen evolution measurements. At pH 5.6, carbonate ions are present in the solution, due to the dissolution of carbon dioxide present in the air. Therefore, the overall corrosion mechanism occurring on the AZ31 surface in NaCl solution is explained by the following reactions:

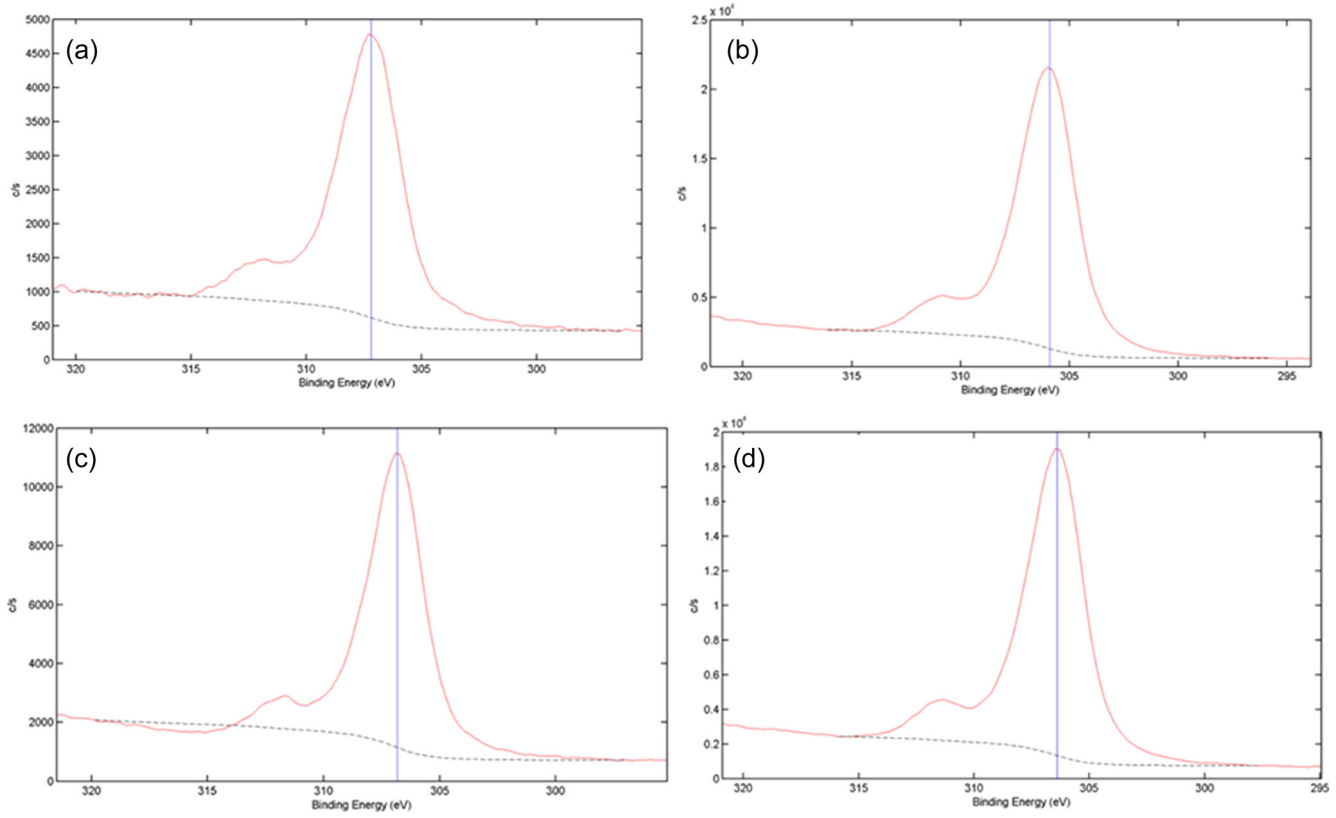

FIGURE 14 Chemical state obtained by X-ray photoelectron spectroscopy analysis of the Mg KLL Auger spectrum for AZ31 exposed for 7 days: (a) to air, (b) 0.1 M NaCl, (c) 0.01 M NaOH, (d) 0.1 M NaCl/0.01 M NaOH. [Color figure can be viewed at wileyonlinelibrary.com]

$$2H^+ + 2e^- \rightarrow H_2, \quad (13)$$

$$2Mg \rightarrow 2Mg^+_{ads} + 2e^-, \quad (14)$$

$$2Mg^+_{ads} + 2H_2O \rightarrow 2Mg^{2+} + H_2 + 2OH^-, \quad (15)$$

$$Mg^{2+} + 2OH^- \rightarrow Mg(OH)_2 \quad (16)$$

$$MgO + H_2O \rightarrow Mg(OH)_2, \quad (17)$$

$$Mg^{2+} + CO_3^{2-} \rightarrow MgCO_3. \quad (18)$$

In an alkaline environment without chloride, EIS measurements highlighted the formation of a protective layer. The modulus at low frequencies is stable with immersion time and the passive oxide is formed on the substrate. The passive layer consists mainly of $Mg(OH)_2$. Nevertheless, the presence of a MgO layer should not be neglected because, despite the very high reactivity of Mg, corrosion is slowed down by this protective layer. The pH decreases to reach a value close to 11. Salgueiro et al.[45] explained that magnesium carbonate can decompose in this pH range and cause slight acidification of the solution. This phenomenon may also explain the absence of magnesium carbonate on the extreme surface of the sample:

$$MgCO_3 + H_2O + OH^- \rightarrow Mg(OH)_2 + HCO_3^-. \quad (19)$$

However, the presence of chloride ions in alkaline media accelerates the dissolution of the magnesium and causes the local degradation of the MgO layer with the formation of filaments appearing in the passive layer. The corrosion current density is in the order of 10^{-5} A/cm^2. The existence of a corrosion product consisting mainly of $Mg(OH)_2$ with a small amount of magnesium carbonate is revealed by XPS. The decrease in pH from 12 to 10 confirms the appearance of carbonate ions by the dissolution of CO_2 in the electrolyte solution and the formation of precipitation products. Finally, the charge transfer resistance is in the order $10^4\ \Omega\,cm^2$ versus immersion time and stable over time. Nevertheless, a significant decrease in charge transfer resistance is observed in the presence of chloride ions in the alkaline solution but the hydrogen production remains quite limited compared to the solution with a lower initial pH even if the same pH is reached after several hours. Despite an alkaline pH, it is important to add in the medium an inhibitor capable of reinforcing the weak passivation layer against chlorides.[25]

Therefore, the overall corrosion mechanism occurring on the AZ31 surface in alkaline solution with chlorides is proposed to the following reactions:

$$2H_2O + 2e^- \rightarrow H_2 + 2\,OH^-, \quad (20)$$

$$Mg \rightarrow Mg^{2+} + 2e^-, \quad (21)$$

$$Mg + 2H_2O \rightarrow Mg^{2+} + H_2 + 2\,OH^-, \quad (22)$$

$$Mg^{2+} + CO_3^{2-} \rightarrow MgCO_3. \quad (23)$$

5 | CONCLUSION

The corrosion mechanism of the AZ31 alloy in three different electrolytes for a duration of 1 week was investigated: an alkaline electrolyte with and without chloride ions as well as an electrolyte with the same chloride content but initially neutral.

The initial pH value is a key parameter in the corrosion progression of AZ31 magnesium alloy. Even if the pH reaches after 1 h is alkaline in each case (close to 11), a pH close to the neutrality at the beginning of immersion destroys the thin MgO layer and leads rapidly to generalized corrosion with a high production of hydrogen. A nonprotective layer of $Mg(OH)_2$ is formed due to its low solubility.

In the initial alkaline solution in the absence of chloride, the protective inner layer of MgO is formed protecting the substrate for a long duration. In the case of chloride ions, the inner protective layer is locally destroyed with the apparition of filiform corrosion after 24 h.

ACKNOWLEDGMENT

The authors wish to thank the 'Région Wallonne' in the framework of the FEDER 2014-2020 program: HYBRITIMESURF.

DATA AVAILABILITY STATEMENT

Data are available on request from the authors.

ORCID

Loic Prince http://orcid.org/0000-0002-4820-7292

REFERENCES

[1] J. F. King, *Mater. Sci. Technol.* **2007**, *23*, 1.
[2] E. Ghali, W. Dietzel, K. U. Kainer, *J. Mater. Eng. Perform.* **2013**, *22*, 2875.
[3] G. Song, A. Atrens, *Adv. Eng. Mater.* **2003**, *5*, 837.
[4] R. M. Asmussen, W. J. Binns, R. Partovi-Nia, P. Jakupi, D. W. Shoesmith, *Mater. Corros.* **2016**, *67*, 39.
[5] F. Cao, G. L. Song, A. Atrens, *Corros. Sci.* **2016**, *111*, 835.
[6] M. Esmaily, M. Shahabi-Navid, J.-E. Svensson, M. Halvarsson, L. Nyborg, Y. Cao, L.-G. Johansson, *Corros. Sci.* **2015**, *90*, 420.
[7] K. Refson, R. A. Wogelius, D. G. Fraser, M. C. Payne, M. H. Lee, V. Milman, *Phys. Rev. B.* **1995**, *52*, 10823.
[8] H. Liu, F. Cao, G.-L. Song, D. Zheng, Z. Shi, M. S. Dargusch, A. Atrens, *Mater. Sci. Technol.* **2019**, *35*, 2003.
[9] S. Thomas, N. V. Medhekar, G. S. Frankel, N. Birbilis, *Curr. Opin. Solid State Mater. Sci.* **2015**, *19*, 85.
[10] G. Baril, N. Pébère, *Corros. Sci.* **2001**, *43*, 471.
[11] M. Esmaily, J. E. Svensson, S. Fajardo, N. Birbilis, G. S. Frankel, S. Virtanen, R. Arrabal, S. Thomas, L. G. Johansson, *Prog. Mater. Sci.* **2017**, *89*, 92.
[12] N. Takeno, *Atlas of Eh-pH Diagrams. Intercomparison of Thermodynamic Databases*, National Institute of Advanced Industrial Science and Technology, Tokyo, Japan **2005**, p. 285. http://scholar.google.com/scholar?hl=en%26btnG=Search%26q=intitle:Atlas%2Bof%2BEh-pH%2Bdiagrams%2BIntercomparison%2Bof%2Bthermodynamic%2Bdatabases#0
[13] H. Hornberger, S. Virtanen, A. R. Boccaccini, *Acta Biomater.* **2012**, *8*, 2442.
[14] S. V. Lamaka, O. V. Karavai, A. C. Bastos, M. L. Zheludkevich, M. G. S. Ferreira, *Electrochem. Commun.* **2008**, *10*, 259.
[15] A. Atrens, G. L. Song, F. Cao, Z. Shi, P. K. Bowen, *J. Magnesium Alloys* **2013**, *1*, 177.
[16] W. A. Badawy, N. H. Hilal, M. El-Rabiee, H. Nady, *Electrochim. Acta* **2010**, *55*, 1880.
[17] H. Yao, Y. Li, A. T. Wee, *Appl. Surf. Sci.* **2000**, *158*, 112.
[18] M. Santamaria, F. Di Quarto, S. Zanna, P. Marcus, *Electrochim. Acta* **2007**, *53*, 1314.
[19] M. Liu, S. Zanna, H. Ardelean, I. Frateur, P. Schmutz, G. Song, A. Atrens, P. Marcus, *Corros. Sci.* **2009**, *51*, 1115.
[20] L. Wang, D. Snihirova, M. Deng, C. Wang, B. Vaghefinazari, G. Wiese, M. Langridge, D. Höche, S. V. Lamaka, M. L. Zheludkevich, *Corros. Sci.* **2021**, *187*, 109501.
[21] A. Pardo, M. C. Merino, A. E. Coy, R. Arrabal, F. Viejo, E. Matykina, *Corros. Sci.* **2008**, *50*, 823.
[22] Z. Shi, M. Liu, A. Atrens, *Corros. Sci.* **2010**, *52*, 579.
[23] G. Song, A. Atrens, D. St John, *Essential Readings in Magnesium Technology*, Springer International Publishing, Cham, Switzerland **2016**, p. 565.
[24] S. V. Lamaka, B. Vaghefinazari, D. Mei, R. P. Petrauskas, D. Höche, M. L. Zheludkevich, *Corros. Sci.* **2017**, *128*, 224.
[25] L. Prince, M. A. Rousseau, X. Noirfalise, L. Dangreau, L. B. Coelho, M. G. Olivier, *Corros. Sci.* **2021**, *179*, 109131.
[26] S. Fajardo, C. F. Glover, G. Williams, G. S. Frankel, *Electrochim. Acta* **2016**, *212*, 510.
[27] S. Feliu, I. Llorente, *Appl. Surf. Sci.* **2015**, *347*, 736.
[28] S. Leleu, B. Rives, J. Bour, N. Causse, N. Pébère, *Electrochim. Acta* **2018**, *290*, 586.
[29] M. P. Gomes, I. Costa, N. Pébère, J. L. Rossi, B. Tribollet, V. Vivier, *Electrochim. Acta* **2019**, *306*, 61.
[30] M. Curioni, L. Salamone, F. Scenini, M. Santamaria, M. Di Natale, *Electrochim. Acta* **2018**, *274*, 343.
[31] G. Baril, C. Blanc, N. Pébère, *J. Electrochem. Soc.* **2001**, *148*, B489.
[32] Y. Zhang, C. Yan, F. Wang, W. Li, *Corros. Sci.* **2005**, *47*, 2816.

[33] F. Cao, Z. Shi, J. Hofstetter, P. J. Uggowitzer, G. Song, M. Liu, A. Atrens, *Corros. Sci.* **2013**, *75*, 78.
[34] G. Song, D. S. T. John, J. Nairn, *Corros. Sci.* **1997**, *39*, 1981.
[35] S. Lebouil, O. Gharbi, P. Volovitch, K. Ogle, *Corrosion* **2015**, *71*, 234.
[36] A. Samaniego, B. L. Hurley, G. S. Frankel, *J. Electroanal. Chem.* **2015**, *737*, 123.
[37] Y. Li, Z. Shi, X. Chen, A. Atrens, *J. Magnesium Alloys* **2021**, *9*, 2049.
[38] P. Zoltowski, *J. Electroanal. Chem.* **1998**, *443*, 149.
[39] M. Pourbaix, *Atlas of Electrochemical Equilibria in Aqueous Solutions*, Pergamon, New York, NY **1966**.
[40] J. Rodriguez, L. Chenoy, A. Roobroeck, S. Godet, M. G. Olivier, *Corros. Sci.* **2016**, *108*, 47.
[41] S. Li, A. C. Bacco, N. Birbilis, H. Cong, *Corros. Sci.* **2016**, *112*, 596.
[42] Z. Shi, A. Atrens, *Corros. Sci.* **2011**, *53*, 226.
[43] S. Feliu, C. Maffiotte, A. Samaniego, J. C. Galván, V. Barranco, *Appl. Surf. Sci.* **2011**, *257*, 8558.
[44] Y. Bouvier, *Surf. Coat. Technol.* **2004**, *180–181*, 169.
[45] M. Salgueiro Azevedo, C. Allély, K. Ogle, P. Volovitch, *Electrochim. Acta* **2015**, *153*, 159.

How to cite this article: L. Prince, X. Noirfalise, Y. Paint, M. Olivier, *Mater. Corros.* **2022**, 1–16. https://doi.org/10.1002/maco.202213116